

PRODUCTION OF THE EXTREME-ULTRAVIOLET LATE PHASE OF AN X CLASS FLARE IN A THREE-STAGE MAGNETIC RECONNECTION PROCESS

Y. DAI^{1,2}, M. D. DING^{1,2}, AND Y. GUO^{1,2}

¹School of Astronomy and Space Science, Nanjing University, Nanjing 210093, China; ydai@nju.edu.cn

²Key Laboratory of Modern Astronomy and Astrophysics (Nanjing University), Ministry of Education, Nanjing 210093, China

Accepted for publication in the Astrophysical Journal Letters

ABSTRACT

We report observations of an X class flare on 2011 September 6 by the instruments onboard the *Solar Dynamics Observatory* (*SDO*). The flare occurs in a complex active region with multiple polarities. The Extreme-Ultraviolet (EUV) Variability Experiment (EVE) observations in the warm coronal emission reveal three enhancements, of which the third one corresponds to an EUV late phase. The three enhancements have a one-to-one correspondence to the three stages in flare evolution identified by the spatially-resolved Atmospheric Imaging Assembly (AIA) observations, which are characterized by a flux rope eruption, a moderate filament ejection, and the appearance of EUV late phase loops, respectively. The EUV late phase loops are spatially and morphologically distinct from the main flare loops. Multi-channel analysis suggests the presence of a continuous but fragmented energy injection during the EUV late phase resulting in the warm corona nature of the late phase loops. Based on these observational facts, We propose a three-stage magnetic reconnection scenario to explain the flare evolution. Reconections in different stages involve different magnetic fields but show a casual relationship between them. The EUV late phase loops are mainly produced by the least energetic magnetic reconnection in the last stage.

Subject headings: Sun: corona — Sun: flares — Sun: UV radiation — Sun: magnetic topology

1. INTRODUCTION

It is widely accepted that flares are a result of the rapid release of magnetic energy stored in the solar corona. Among the radiative output from a flare, emission from the Extreme-Ultraviolet (EUV) spectral range covers a substantial fraction, thus serving as an important tool to diagnose the dynamics and evolution of the flare. Observations of the Sun in EUV have been carried out for more than half a century (e.g., Friedman 1963). However, previous observations often suffered from the limited spectral range. The situation has been greatly improved since the recently launched *Solar Dynamics Observatory* (*SDO*; Pesnell et al. 2012) mission provides both spectroscopic observations with full EUV spectral coverage and simultaneous imaging observations in multiple EUV bandpasses.

One of the intriguing phenomena discovered by *SDO* is an “EUV late phase” in some flares (Woods et al. 2011), which is seen as a second peak in the warm coronal (~ 3 MK) emissions (such as Fe xvii) several minutes to a few hours after the *GOES* soft X-ray (SXR) peak. There are, however, no significant enhancements of the SXR or hot coronal (~ 10 MK) emissions in the EUV late phase, and spatially-resolved observations show that the secondary warm coronal emission comes from a set of longer loops rather than the original flaring loops. Up to now, there are only a few reports of the EUV late phase in literatures, and the origin of the EUV late phase is still not fully understood. Some authors thought that the EUV late phase is due to a second energy injection late in the flare (e.g., Woods et al. 2011; Hock et al. 2012b), while others proposed that it is mainly a cooling-effect extending from the initial main flare heating (e.g., Liu et al. 2013). To clarify this question, in this Letter we present

SDO observations of an X class flare on 2011 September 6, which exhibits an extended EUV late phase. Based on the observational facts found in this flare, we propose a specific scenario, three-stage magnetic reconnection, to explain the production of the EUV late phase.

2. OBSERVATIONS AND DATA ANALYSIS

We use data from the three instruments onboard *SDO*. The EUV Variability Experiment (EVE; Woods et al. 2012) measures full-disk integrated EUV irradiance from 0.1 to 105 nm with 0.1 nm spectral resolution and 10 s temporal cadence. The EVE data used in this study are primarily from the MEGS-A channel (Hock et al. 2012a), which covers the 7–37 nm wavelength range with a nearly 100% duty cycle. The Atmospheric Imaging Assembly (AIA; Lemen et al. 2012) provides simultaneous full-disk images of the transition region and corona in 10 channels with 1''5 spatial resolution and 12 s temporal resolution. In addition, magnetograms from the Helioseismic and Magnetic Imager (HMI; Scherrer et al. 2012) are chosen to check the magnetic topology of the flare.

The flare under study occurred in NOAA active region (AR) 11283 on 2011 September 6, positioned close to the disk center. It is an X2.1 class flare that started at 22:12 UT, peaked around 22:21 UT, and ended at 22:24 UT, as revealed by the *GOES* 0.1–0.8 nm light curve in Figure 1.

To study the thermal evolution of the flare, in Figure 1 we also plot the time profiles of the background-subtracted irradiance in six EVE spectral lines, which cover temperatures from $\log T \sim 4.9$ to $\log T \sim 7$. The flare exhibits the all four characteristics pointed out in Woods et al. (2011). First, the cold chromospheric He II 30.4 nm emission showed an impulsive enhancement and peaked around 22:19 UT, almost coincident with the

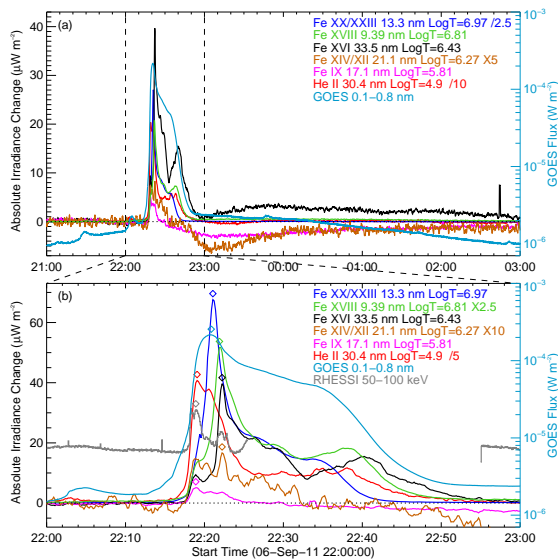


FIG. 1.— Time profiles of the background-subtracted irradiance in six *SDO*/*EVE* spectral lines and *GOES* 0.1–0.8 nm flux for the 2011 September 6 X2.1 flare. Panel (a) shows the whole evolution of the flare, during which the warm coronal Fe XVI 33.5 nm emission exhibits an extended late phase lasting until the first few hours of 2011 September 7. Panel (b) gives an enlarged view of the flare evolution between 22:00 UT and 23:00 UT, with the *RHESSI* 50–100 keV count rate over-plotted. The color-coded diamonds denote the peak time for the corresponding emission.

RHESSI 50–100 keV hard X-ray (HXR) emission peak, as well as the spikes in the emissions from Fe IX to Fe XVI. This implies that the chromosphere, as responding to impact of the non-thermal electrons accelerated during the flare’s impulsive phase, was instantly heated to $\log T \sim 6.4$ (Milligan et al. 2012; Chamberlin et al. 2012). Second, the hot coronal Fe XX/XXIII 13.3 nm emission closely resembled the *GOES* SXR time series and peaked around 22:21 UT, which is believed to be a result of the chromospheric evaporation caused by the initial heating. The cooler emissions then peaked sequentially with decreasing temperatures within a short period of 70 s, revealing a fast cooling rate over 1×10^5 K s⁻¹. Third, the cool coronal Fe IX 17.1 nm and moderately warm coronal Fe XIV/XII 21.1 nm emissions decreased after the peak of the main phase and turned into a coronal dimming. A coronal mass ejection (CME) was observed being associated with the flare, and the coronal dimming is most likely to reflect the mass drainage during the CME launch (e.g., Aschwanden et al. 2009). Fourth, as the dimming in cool coronal emissions developed and other emissions returned to the pre-flare level, the warm coronal Fe XVI 33.5 nm emission showed another small enhancement that started from $\sim 23:00$ UT and lasted until the first few hours of 2011 September 7. It should correspond to the EUV late phase as defined in Woods et al. (2011), which will be further validated by the aftermentioned AIA imaging observations. Note that in this late phase there was also likely a very weak increase in the moderately hot coronal Fe XVIII 9.39 nm emission.

Besides these four features, we find that additional moderate enhancements in the *EVE* 30.4, 33.5, and 9.39 nm emissions were seen to start from $\sim 22:33$ UT and peak around 22:40 UT. The *EVE* 13.3 nm emission and the *GOES* SXR flux also showed a hump during this

period. Therefore, compared to the typical EUV late phase as demonstrated in Woods et al. (2011), which is directly preceded by the flare’s main phase, in this flare there is another “intermediate phase” characterized by the moderate peak between the main phase and the late phase.

Spatially-resolved AIA observations of the flare evolution in six coronal channels are presented in the online animation. Figure 2 shows some snapshots of the animation in the AIA 33.5 and 17.1 nm channels, respectively, as well as a light-of-sight (LOS) magnetogram of AR 11283 taken at 22:14 UT by HMI. Three main polarities are identified and labeled as P1, N1, and P2, among which P2 is a parasitic positive polarity embedded in the negative polarity N1. The flare first occurred along the southeastern part of the polarity inversion line (PIL) between N1 and P2, behaving as a sigmoid-to-flux-rope eruption pattern (cf, Liu et al. 2010), which is best seen in AIA 13.1 and 9.4 nm. Note that prior to the event a semi-circular filament was observed to lie along the PIL, the southern part of which has been successfully modeled as a flux rope (FR) by Feng et al. (2013) and Jiang et al. (2013) by using different nonlinear force-free field (NLFFF) extrapolation methods. From $\sim 22:18$ UT the FR started to rise rapidly, with the flare ribbons becoming more elongated along the PIL and the outer one eventually turning into a circular ribbon (Figures 2(a) and (e)). Following the brightening of the main flare ribbons, a remote flare ribbon appeared in P1, over a distance of 80'' east of the main flare region. The situation is very similar to those studied in Masson et al. (2009) and Wang & Liu (2012), indicating the presence of a 3D null-point magnetic topology, which is also expected from the LOS magnetogram. Afterwards, the region on the eastern side of the remote ribbon quickly turned into a coronal dimming that persisted during the whole evolution of the flare.

This first stage eruption was followed by a second stage eruption, which was seen as the continuous ejection of cold material from the northern part of the filament starting from $\sim 22:33$ UT (Figures 2(b) and (f)). This moderate ejection produced new post-flare loops mainly on its southern side rather than centered on the filament itself. In AIA 13.1 and 9.4 nm (see online animation), there appeared a second set of longer but less prominent loops connecting the eastern side of the filament (in N1) and the abovementioned remote flare ribbon (in P1), which were not visible in the cooler coronal channels at that moment.

The second stage eruption lasted about 30 minutes. As the post-flare loops in the main flare region cooled down, longer post-flare loops connecting N1 and P1 became more and more dominant in particular in the warm and cool coronal channels. The appearance of these loops coincided with the enhancement in the *EVE* Fe XVI 33.5 nm emission starting from $\sim 23:00$ UT, and the loops were spatially distinct from the original post-flare loops, further supporting the identification of an EUV late phase for this third stage evolution. These late phase loops were first localized at the same location of the second set of loops previously only seen in the hotter coronal channels during the second stage (Figures 2(c) and (g)), later became more spatially spread (Figure 2(h)). As noted in Woods et al. (2011), the late phase loops are very diffuse

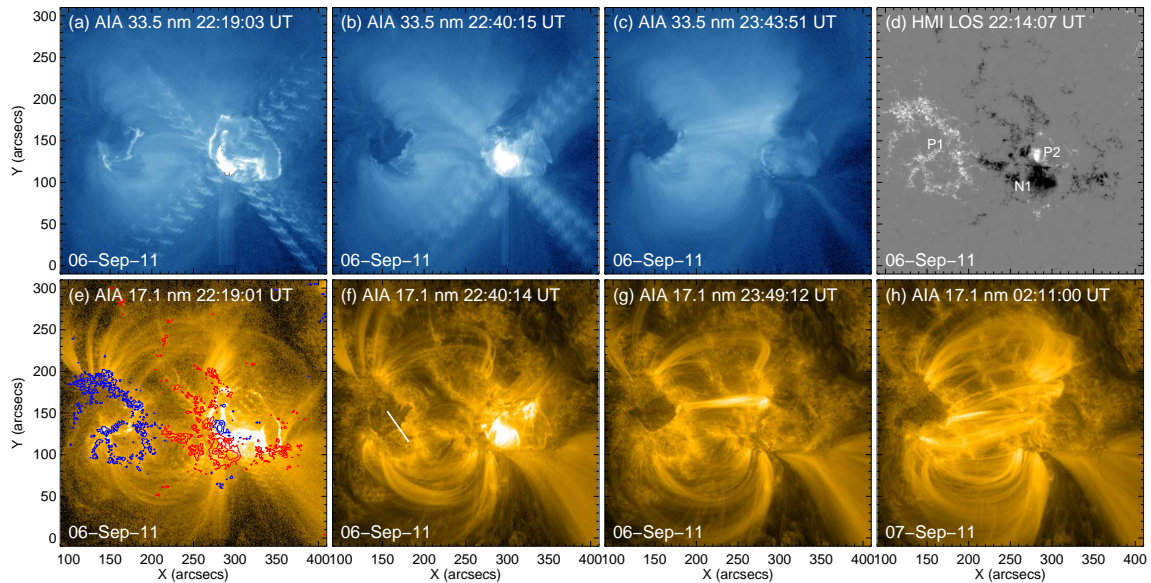


FIG. 2.— Snapshots of the flare evolution taken by *SDO/AIA* at 33.5 nm (a–c) and 17.1 nm (e–h), as well as a light-of-sight (LOS) magnetogram of AR 11283 taken at 22:14 UT by *SDO/HMI* (d). Three main polarities are identified and labeled as P1, N1, and P2, whose contours are also overlaid in panel (e). A slice is placed in panel (f), along which the evolution will be traced in Figure 3.

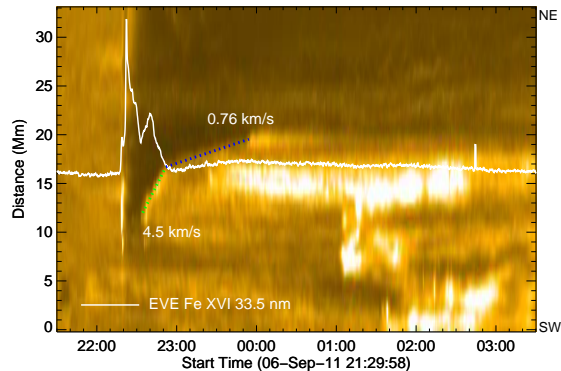


FIG. 3.— Base ratio time-distance diagram of the AIA 17.1 nm images along the slice in Figure 2(f), showing the eastward (dimming-ward) expansion of the remote flare ribbon. The transition of the expansion velocity from 4.5 km s^{-1} (green dotted line) to 0.76 km s^{-1} (blue dotted line) coincides with the over-plotted EVE 33.5 nm emission variation (white solid line).

in morphology in the warm coronal AIA 33.5 nm channel, but quite distinct in the cool coronal channels such as AIA 17.1 nm.

It is worth noting that the remote flare ribbon brightened again and showed a long-lasting eastward (dimming-ward) expansion starting from the second stage eruption when long loops were found to anchor on it. This is an indicator of progressive magnetic reconnection according to the standard flare model. In Figure 2(f) we place a slice roughly perpendicular to the remote ribbon to trace its movement in AIA 17.1 nm. Because of the low brightness of the remote ribbon, we simply use linear fit to track the ribbon expansion. As revealed in Figure 3, the expansion velocity of the remote ribbon turned from 4.5 km s^{-1} to 0.76 km s^{-1} , coinciding with the transition from the second stage to the third stage, and also consistent with the evolution of the EVE 33.5 nm emission. The expansion velocities are considerably lower than those in some typical two-ribbon flares, which are several tens of km s^{-1} (e.g., Asai et al. 2004; Miklenic et al. 2007), implying less and less ener-

getic magnetic reconnections during the second and third stages with much lower reconnection rates than the main flare reconnection.

The AIA base difference images in Figure 4 highlight the flare’s three-stage evolution more clearly. To determine the contribution of different parts of the AR to the flare emission, we identify three regions, which are indicated by the color boxes in the AIA 33.5 nm images, and calculate the light curve by summing the count rate over all pixels in each region. The red box represents the main flare region, the blue one outlines the outer loop region, which is believed to account for the EUV late phase, and the black one surrounds the full AR. We plot the background-subtracted AIA light curves in 33.5 nm from the three regions in Figure 4(g), and compare the AIA 33.5 nm full AR light curve with the EVE 33.5 nm profile in Figure 4(h). First, the general similarity between the two profiles in Figure 4(h) suggests that the change in the EVE full-disk integrated irradiance comes mainly from the AR. Actually, there was no other major activity on the visible disk during the period of this event. Second, as expected, emission from the main flare region dominates in the main phase and the intermediate phase, while the outer loop region is responsible for the late phase. Note that in the main and intermediate phases there were also some intensity increases from the outer loop region, which we attribute to the brightening of the remote flare ribbon and CCD-bleed interference stripes extending from the intensively flaring site.

To study the thermal evolution the EUV late phase loops, we select a sub-region defined by the white parallelogram in Figure 4(f), which includes the most prominent late phase loops seen in AIA 33.5 nm, and calculate the intensity variability in six AIA coronal channels for this region. As revealed in Figure 4(i), the EUV late phase can be decomposed into many episodes; each episode is characterized by a cooling process, with the emissions peaking sequentially with decreasing temperatures. Furthermore, combined with the imaging observations, it is found that these multiple peaks appear to be

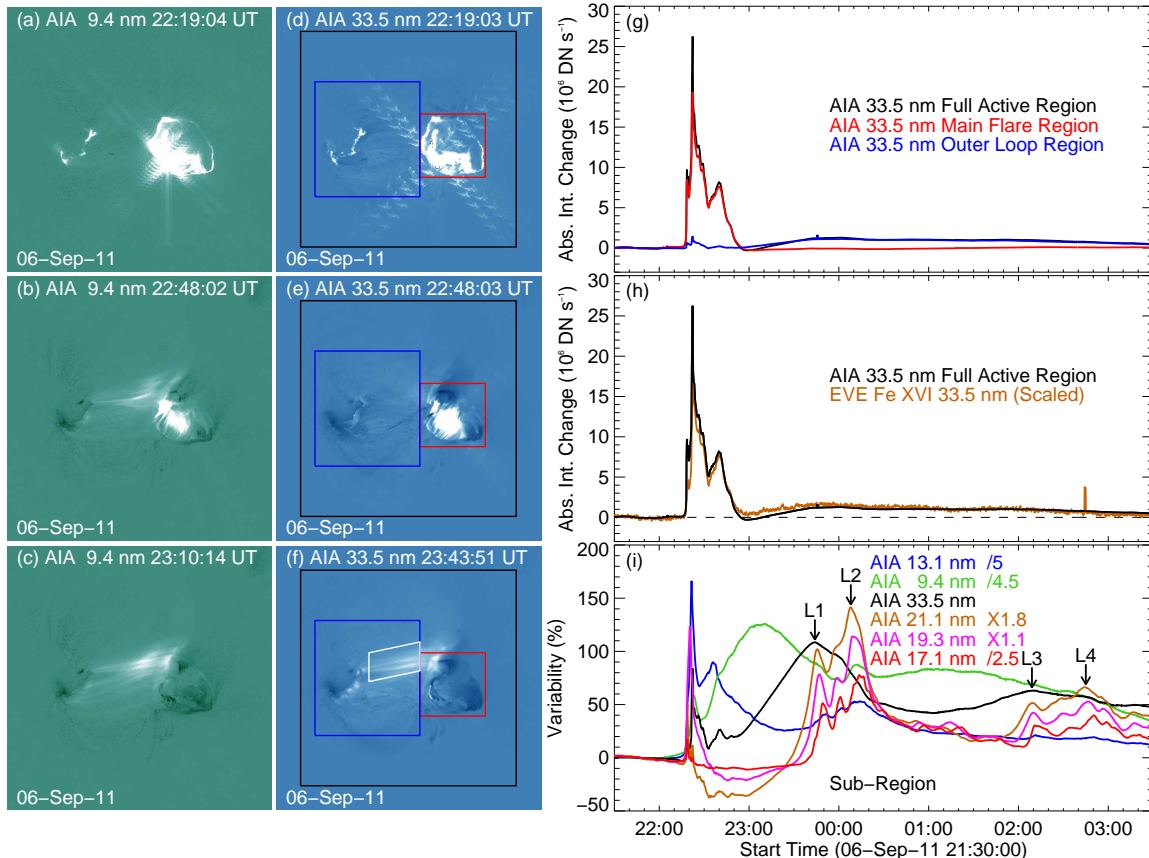


FIG. 4.— Left and middle: AIA base difference images of the flare at 9.4 and 33.5 nm, respectively. In the right, from top to bottom: AIA 33.5 nm light curves from regions indicated by the color boxes in the AIA 33.5 nm images, comparison between the AIA 33.5 nm full AR light curve and the EVE 33.5 nm profile, and intensity variability in six AIA coronal channels for the sub-region of the late phase loops defined by the white parallelogram in panel (f). Here the variability is defined as the relative change from the background. Four episodes in the late phase are picked up by the arrows in panel (i) and labeled as L1–L4.

related to different, but adjacent, late phase loops cooling into the corresponding emission temperature ranges at different times, in particular in the cool coronal channels. This indicates the presence of a continuous, but fragmented both temporally and spatially, energy injection during the EUV late phase, challenging the conclusion of Liu et al. (2013) that the appearance of the late phase loops is mainly a cooling-effect rather than the result of a later energy injection. We pick up four most prominent episodes labeled as L1–L4, and list the time of peak emission seen in six AIA channels for each episode in Table 1. It is seen that in L2 the AIA 9.4 nm peak follows the AIA 19.3 nm peak, and all detectable peaks in AIA 13.1 nm are delayed from the corresponding AIA 17.1 nm peaks. This behavior can be expected from the AIA temperature response functions (TRFs) calculated using the latest CHIANTI atomic database (Landi et al. 2013), which also show a second cool coronal peak at $\log T \sim 6.0$ for AIA 9.4 nm and $\log T \sim 5.8$ for AIA 13.1 nm, and suggests the warm corona nature of the late phase loops. Between L2 and L3 the variabilities in AIA 9.4 and 33.5 nm showed opposite patterns, further suggesting that during this period the AIA 9.4 nm channel is mainly sensitive to cool late phase loops that cool from warm coronal temperatures. L1 is a little bit special, in which the appearance of the late phase loops in AIA 33.5 nm (Figure 4(f)) is a combined effect of the cooling from the hotter AIA 9.4 nm loops (Figure 4(c)) and the late

phase energy injection. The cooling rates in these four episodes are $0.3\text{--}1.2 \times 10^4 \text{ K s}^{-1}$, orders of magnitude lower than that in the main phase derived from the EVE observations.

3. DISCUSSION AND CONCLUSION

The 2011 September 6 X2.1 flare conforms to the criteria for an EUV late phase flare defined in Woods et al. (2011). To our knowledge, this may be the first report of the EUV late phase of a flare above the X class. The ratio of the late phase peak to the main phase peak is only 9.4%, significantly lower than those in Woods et al. (2011). We attribute this low ratio to the intense energy injection during the impulsive phase, which causes a strong main phase peak of $\sim 100\%$ above the background.

According to previous studies, the multipolar magnetic fields may be a necessary condition for the production of an EUV late phase (e.g., Hock et al. 2012b; Liu et al. 2013). We propose a three-stage magnetic reconnection scenario to explain the flare evolution under such a magnetic topology.

The main flare reconnection between N1 and P2 is triggered by the tether-cutting mechanism (Moore et al. 2001), as evidenced by the sigmoid-to-flux-rope eruption pattern. The appearance of the remote flare ribbon may suggest a secondary null-point reconnection (Masson et al. 2009; Reid et al. 2012). A magnetic null-point was indeed found by Jiang et al. (2013), but the

TABLE 1
TIME OF THE PEAK EMISSION IN AIA FOR THE SELECTED EPISODES IN THE LATE PHASE

Channel (nm)	Ion	log T	Peak Time (UT)			
			L1 (6-Sep)	L2 (7-Sep)	L3 (7-Sep)	L4 (7-Sep)
9.4 (hot)	Fe XVIII	6.8	23:10:14
33.5	Fe XVI	6.4	23:43:51	...	02:09:27	...
21.1	Fe XIV	6.3	23:45:48	00:07:48	02:09:24	02:45:48
19.3	Fe XII	6.1	23:46:55	00:09:19	02:09:55	02:48:31
9.4 (cool)	Fe X	6.0	...	00:12:02
17.1	Fe IX	5.9	23:49:12	00:13:36	02:11:00	02:50:24
13.1 (cool)	Fe VIII	5.8	23:51:21	00:13:45	02:11:21	...

outer spine field lines surrounding the null-point extend to the northwest rather than the eastern remote ribbon. Nevertheless, large-scale overlying field lines that connect P1 and N1 do exist. When the FR erupts, it strongly reconnects with and stretches these overlying field lines, causing the brightening of the remote ribbon and deep dimming at the far side of the remote ribbon. This FR-driven reconnection should belong to the breakout reconnection (Antiochos et al. 1999).

The eruption of the FR largely removes the overlying magnetic confinement. Therefore, the northern part of the filament starts to rise as a sequence of the torus instability (Kliem & Török 2006). The rising filament also drives the breakout reconnection but in a gentle manner, producing two sets of side-lobe post-flare loops (Figure 4(b)). Since the southern side-lobe loops located in the main flare region are more closer to the reconnection site, they are more prominent than the northeastern ones, responsible for the flare’s intermediate phase.

As the filament-driven breakout reconnection turns the lower overlying field lines into side lobes, new reconnection occurs between the higher overlying field lines that are previously stretched. The process is similar to the main flare reconnection, but is much less energetic because of the weaker magnetic fields that are involved. Hence the reconnection only produces moderately heated warm EUV late phase loops (Figure 4(f)). These loops cool as they retract, sequentially brightening in cooler coronal channels. Meanwhile, the whole AR gradually recovers to its pre-flare state. In a large-scale extent, the on-going reconnection can occur at different sites and with different rates, making the energy injection rather fragmented. The slow cooling rates for the late phase loops can be expected from their long length (cf.

Cargill et al. 1995).

The three-stage magnetic reconnections show a casual relationship between each other, and the EUV late phase is mainly a production of the third stage reconnection. It is believed that some very early late phase loops (see Figure 4(b)) have already been produced during the second stage breakout reconnection (Hock et al. 2012b). The loops are not visible in cooler coronal channels just because they are still relatively hot at that moment.

The diffuse morphology of the late phase loops seen in AIA 33.5 nm images is also reflected from the more smooth AIA 33.5 nm profile, as compared with the less smooth cooler emission profiles shown in Figure 4(i). Woods et al. (2011) attribute this phenomenon to the relatively slow cooling rate at warm coronal temperatures compared to that at cooler coronal temperatures. However, it seems not to be the case for the current event as revealed in Table 1. We present an alternative explanation in terms of the AIA TRFs. The AIA 33.5 nm TRF is quite flat from the peak with decreasing temperatures. It means that as a warm late phase loop cools its visibility in AIA 33.5 nm does not change much; therefore, there could be many overlapping loops visible at the same time. Nevertheless, the TRFs for the cooler coronal channels (AIA 21.1, 19.3, and 17.1 nm) have a sharp peak. In these channels, a small change of the loop temperature around the TRF peak will significantly change the loop intensity, resulting in the sharp loop morphology and the large fluctuation of the intensity profile.

We are grateful to the anonymous referee for his/her insightful comments. This work is supported by NSFC (11103009, 10933003, 11203014, and 11078004), and by 973 project of China (2011CB811402). *SDO* is a mission of NASA’s Living With a Star (LWS) program.

REFERENCES

- Antiochos, S. K., DeVore, C. R., & Klimchuk, J. A. 1999, *ApJ*, 510, 485
- Asai, A., Yokoyama, T., Shimojo, M., et al. 2004, *ApJ*, 611, 557
- Aschwanden, M. J., Nitta, N. V., Wuelsel, J.-P., et al. 2009, *ApJ*, 706, 376
- Cargill, P. J., Mariska, J. T., & Antiochos, S. K. 1995, *ApJ*, 439, 1034
- Chamberlin, P. C., Milligan, R. O., & Woods, T. N. 2012, *Sol. Phys.*, 279, 23
- Feng, L., Wiegmann, T., Su, Y., et al. 2013, *ApJ*, 765, 37
- Friedman, H. 1963, *ARA&A*, 1, 59
- Hock, R. A., Chamberlin, P. C., Woods, T. N., et al. 2012a, *Sol. Phys.*, 275, 145
- Hock, R. A., Woods, T. N., Klimchuk, J. A., Eparvier, F. G., & Jones, A. R. 2012b, *ArXiv:1202.4819*
- Jiang, C., Feng, X., Wu, S. T., & Hu, Q. 2013, *ApJ*, 771, L30
- Kliem, B., & Török, T. 2006, *Physical Review Letters*, 96, 255002
- Landi, E., Young, P. R., Dere, K. P., Del Zanna, G., & Mason, H. E. 2013, *ApJ*, 763, 86
- Lemen, J. R., Title, A. M., Akin, D. J., et al. 2012, *Sol. Phys.*, 275, 17
- Liu, K., Zhang, J., Wang, Y., & Cheng, X. 2013, *ApJ*, 768, 150
- Liu, R., Liu, C., Wang, S., Deng, N., & Wang, H. 2010, *ApJ*, 725, L84
- Masson, S., Pariat, E., Aulanier, G., & Schrijver, C. J. 2009, *ApJ*, 700, 559
- Miklenic, C. H., Veronig, A. M., Vršnak, B., & Hanslmeier, A. 2007, *A&A*, 461, 697
- Milligan, R. O., Chamberlin, P. C., Hudson, H. S., et al. 2012, *ApJ*, 748, L14

- Moore, R. L., Sterling, A. C., Hudson, H. S., & Lemen, J. R. 2001, *ApJ*, 552, 833
- Pesnell, W. D., Thompson, B. J., & Chamberlin, P. C. 2012, *Sol. Phys.*, 275, 3
- Reid, H. A. S., Vilmer, N., Aulanier, G., & Pariat, E. 2012, *A&A*, 547, A52
- Scherrer, P. H., Schou, J., Bush, R. I., et al. 2012, *Sol. Phys.*, 275, 207
- Wang, H., & Liu, C. 2012, *ApJ*, 760, 101
- Woods, T. N., Hock, R., Eparvier, F., et al. 2011, *ApJ*, 739, 59
- Woods, T. N., Eparvier, F. G., Hock, R., et al. 2012, *Sol. Phys.*, 275, 115